Proceedings of the ASME 2011 Dynamic Systems and Control Conference
DSCC2011
October 31 - November 2, 2011, Arlington, VA, USA

DSCC2011-6142

NONLINEAR CONTROL OF VARIABLE SPEED WIND TURBINES WITH SWITCHING ACROSS OPERATING REGIMES

Tuhin Das*
Mechanical Engineering Dept.
Rochester Institute of Technology
Rochester, NY 14623
Email: tkdeme@rit.edu

Greg Semrau
Mechanical Engineering Dept.
Rochester Institute of Technology
Rochester, NY 14623

Sigitas Rimkus
Mechanical Engineering Dept.
Rochester Institute of Technology
Rochester, NY 14623

ABSTRACT

One of the key control problems associated with variable speed wind turbine systems is maximization of energy extraction when operating below the rated wind speed and power regulation when operating above the rated wind speed. In this paper, we approach these problems from a nonlinear systems perspective. For below rated wind speeds we adopt existing work appearing in the literature and provide further insight into the characteristics of the resulting equilibrium points of the closed-loop system. For above rated wind speeds, we propose a nonlinear controller and analyze the stability property of the resulting equilibria. We also propose a method for switching between the two operating regimes that ensures continuity of control input at the transition point. The control laws are verified using a wind turbine model with a standard turbulent wind speed profile that spans both operating regimes.

NOMENCLATURE

P Extracted aerodynamic power, W
ρ Density of air, kg/m^2
R_r Rotor radius, m
A Swept area of rotor ($=\pi R_r^2$), m^2
V_w Wind velocity, m/s
C_p Rotor efficiency
β Blade pitch, rad
λ Tip speed ratio
$\dot{\theta}_r$, $\dot{\theta}_g$ Rotor and generator angular speeds, rad/s
J_r, J_g Rotor and generator inertia, $kg\,m^2$
D_r, D_g Damping of rotor and generator inertia, $kg\,m^2/s$
D_{ls}, D_{hs} Damping of rotor and generator shafts, $kg\,m^2/s$
K_{ls}, K_{hs} Spring constants of rotor and generator shafts, $kg\,m^2/s^2$
T_r, T_g Rotor and generator torques, $kg\,m^2/s^2$
GR Gearbox transmission ratio
V_g, i_g, R_g Generator voltage, current and resistance, V, A, Ω
K_v, K_i Generator back e.m.f and torque constants, Vs, Nm/A

INTRODUCTION

With the growing energy demand and need to decrease greenhouse gas emissions, renewable energy systems are poised to become a large part of energy generation. One of the most popular renewable energy systems over the past decade has been the wind turbine. Technological advances in modeling, prediction, sensing and control combined with the current shift towards decentralized power have prompted development of wind energy systems. Although initial expenditures could be an issue, the overall costs of installing and running wind turbines are rapidly reducing with technological advances [1]. There are two different main types of wind turbines, horizontal axis and vertical axis wind turbines [1, 2]. The focus of this work in on horizontal axis wind turbines (HAWTs). There are two primary classifications of HAWTs, fixed speed and variable speed. The fixed speed system is easy to build and operate but variable speed system provides greater energy extraction, up to a 20% increase over fixed speed [1]. The variable speed system on the other hand requires more sophisticated controllers, which is an area of active research [3].

From a systems perspective, energy is injected into the turbine through the torque generated at the turbine rotor due to wind velocity. Energy is extracted by drawing current from the generator, which effectively provides a braking torque. In addition,

*Address all correspondence to this author.

the amount of wind energy extracted can be modulated by varying the pitch angles of the rotor blades. The generator torque (or current draw) and the blade pitch angle can be considered as control inputs. A variable speed wind turbine operates differently in different operating regimes, as shown in Fig.3, see [4, 5]. These operating regimes are explained in detail in the section titled Operating Regimes. The main regimes of operation are, below rated wind speed (regime 2, Fig.3) and above rated wind speed (regime 3, Fig.3). A significant amount of work has been reported in the literature for regime 2 operation where maximization of the extracted power is the main objective [5–9]. Typical control designs maintain the wind turbine at a specific optimal operating point. In scenarios where this operating point may not be exactly known or could change with time, it is adaptively identified using an augmented parameter estimation algorithm.

Control designs proposed for regime 3 operations are relatively fewer in the literature. In [10], the authors propose a cascaded generator torque controller. In both [3] and [11], the authors propose multi-variable control in regime 3, employing both blade pitch and generator torque as control inputs. Here the objective is to maintain relatively uniform generator torque and thereby maintain uniform rotor speeds while achieving power regulation. As control algorithms for the two regimes are considerably different, switching between controllers must be handled carefully. There is very limited amount of work in the literature that addresses the switching aspect. In [11], the authors propose a transition method that interpolates between their regime 2 and 3 generator control torques, based on the current rotor speed.

In this paper, we address the control of a variable speed wind turbine from a nonlinear systems perspective. For regime 2 operation, we do not attempt to develop a new control algorithm. However, with the controller of [5] as a baseline algorithm, we provide further insight into the characteristics of the equilibrium points and obtain a limiting operating point. For regime 3 operation, we propose a simple nonlinear control and investigate the stability of the equilibrium. As in regime 2, the proposed regime 3 controller also results in two equilibrium points, of which one is stable and the other is unstable. We further determine the region of attraction of the stable equilibrium point. We next propose a method for switching between controllers based on rotor speed that ensures continuity of rotor speed at the transition point. The paper is organized as follows. First the system model is described. This is followed by a discussion on control development where we first discuss the operating regimes and then present the control algorithms for regimes 2 and 3. Switching between regimes is discussed next. Simulation results are next provided and finally concluding remarks are presented.

SYSTEM MODEL

The power extracted from a wind turbine is given by [2]

$$P = \frac{1}{2}\rho A C_p(\beta, \lambda) V_w^3 \tag{1}$$

The rotor efficiency C_p is dependent on two factors, blade pitch β, and tip speed ratio λ. The tip speed ratio is defined as follows

$$\lambda = \frac{\dot{\theta}_r R_r}{V_w} \tag{2}$$

In Fig.1, a sample rotor efficiency surface is given. Fig.2 gives a

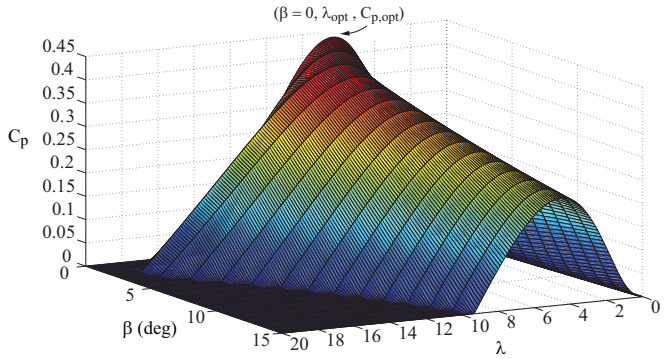

Figure 1. ROTOR EFFICIENCY CURVES AS A FUNCTION OF TIP SPEED RATIO AND BLADE PITCH ANGLE

schematic view of the mechanical system. Assuming the inertia of the gear box to be negligible, we have the following equations of motion:

$$\begin{gathered} J_r\ddot{\theta}_r + D_{ls}\left(\dot{\theta}_r - \dot{\theta}_{gb,1}\right) + K_{ls}\left(\theta_r - \theta_{gb,1}\right) + D_r\dot{\theta}_r = T_r \\ J_g\ddot{\theta}_g + D_{hs}\left(\dot{\theta}_g - \dot{\theta}_{gb,2}\right) + K_{hs}\left(\theta_g - \theta_{gb,2}\right) + D_g\dot{\theta}_g = -T_g \\ D_{ls}\left(\dot{\theta}_r - \dot{\theta}_{gb,1}\right) + K_{ls}\left(\theta_r - \theta_{gb,1}\right) = T_{gb,1} \\ D_{hs}\left(\dot{\theta}_g - \dot{\theta}_{gb,2}\right) + K_{hs}\left(\theta_g - \theta_{gb,2}\right) = -T_{gb,2} \\ GR = T_{gb,1}/T_{gb,2} = \dot{\theta}_{gb,2}/\dot{\theta}_{gb,1} = \theta_{gb,2}/\theta_{gb,1} \end{gathered} \tag{3}$$

From Eq.(3), we have

$$\begin{gathered} J_r\ddot{\theta}_r = T_r - T_{gb,1} - D_r\dot{\theta}_r, \quad J_g\ddot{\theta}_g = -T_g + T_{gb,2} - D_g\dot{\theta}_g, \\ \Rightarrow \quad \left[J_r\ddot{\theta}_r + GR\, J_g\ddot{\theta}_g\right] = T_r - GR\, T_g - \left[D_r\dot{\theta}_r + GR\, D_g\dot{\theta}_g\right] \end{gathered} \tag{4}$$

The electrical generator is modeled as a static power conversion device with a conversion efficiency incorporated through resistive losses, as follows:

$$V_g = K_v\dot{\theta}_g - i_g R_g, \quad T_g = K_i i_g \tag{5}$$

CONTROL DEVELOPMENT

Operating Regimes

The operating regimes of a wind turbine are shown in Fig. 3. In regime 1, the wind energy is not sufficient compared to the

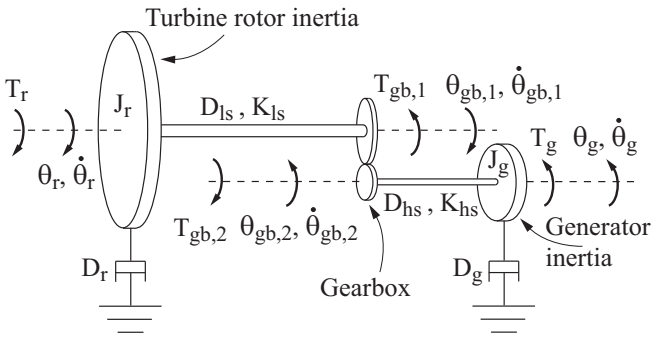

Figure 2. DRIVE TRAIN MODEL WITH A GEAR BOX

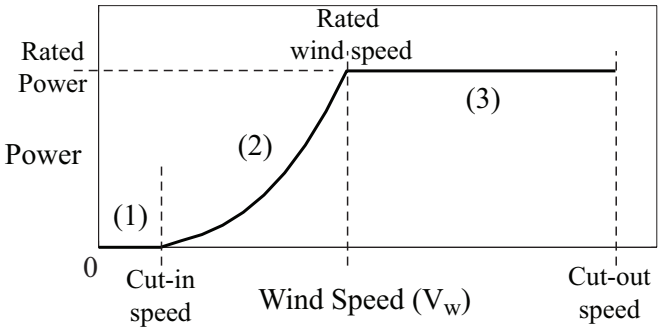

Figure 3. OPERATING REGIMES OF VARIABLE SPEED WIND TURBINE

system component efficiencies to generate net power. Regime 2 is between the cut-in speed and the rated wind speed. Here, the wind turbine is operated under constant C_p. To maximize power, C_p is maintained near its maximum (optimum) value. This optimal operating point is indicated by $C_{p,opt}$ in Fig.3. The wind turbine operates in regime 3 for wind speeds between the rated speed and the cut-out speed. Here, for mechanical and electrical safety, the power capture is limited. The wind turbine operates at constant power mode, delivering the rated power. This is achieved by progressively decreasing C_p as the wind speed increases. Beyond the cut-out speed, operation is deliberately stalled to prevent damage. Stall is achieved by proper blade design or by using a braking clutch or by modulating the blade pitch.

Below Rated Wind Speed - Regime 2

As discussed in the Introduction, control design for regime 2 is thoroughly addressed in the literature. We do not attempt to develop a new control design for this regime. Rather, we focus on the stability analysis of the closed loop system. First, a commonly used simplified form of Eq.(4) is obtained by neglecting the compliance between θ_r and θ_g,

$$J_e\ddot{\theta}_r = T_r - GR\,T_g - D_e\dot{\theta}_r,\; J_e \triangleq J_r + GR^2 J_g,\; D_e \triangleq D_r + GR^2 D_g \tag{6}$$

Another simplification commonly appearing in literature is to neglect $D_e\dot{\theta}_r$ in Eq.(6), due to its relatively small magnitude in comparison to T_r or $GR\,T_g$. This gives

$$J_e\ddot{\theta}_r = T_r - GR\,T_g \tag{7}$$

A standard control strategy for regime 2 operation is

$$GR\,T_g = k_t^*\dot{\theta}_r^2, \quad k_t^* > 0 \tag{8}$$

For constant wind speeds, the closed-loop system is

$$\dot{\lambda} = \frac{\rho AR^2 V_w}{2J_e}\left(\frac{C_p}{\lambda^3} - \frac{2k_t^*}{\rho AR^3}\right)\lambda^2, \tag{9}$$

The stability of the above closed-loop system is studied extensively in [5]. The authors prove that if the curve

$$C_p = \frac{2k_t^*}{\rho AR^3}\lambda^3 \tag{10}$$

intersects the $C_p - \lambda$ curve at points λ_1 and λ_2, as shown in Fig.4, then the equilibrium point $\left(C_p^*, \lambda_*\right)$, where $\lambda_* = \lambda_2$ and $C_p^* =$

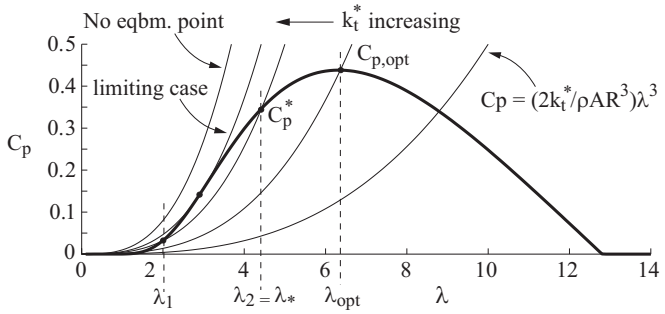

Figure 4. EQUILIBRIUM POINTS FOR BELOW RATED WIND SPEED UNDER CONTROL LAW EQ.(8)

$2k_t^*\lambda_*^3/\rho AR^3$, is asymptotically stable with a region of attraction of $\lambda \in (\lambda_1, \infty)$. We directly adopt this control strategy for regime 2 operation.

There is a permissible range of k_t^* where stability of the equilibrium $\left(C_p^*, \lambda_*\right)$ is guaranteed. From Fig.4 and Eq.(10), we observe that as k_t^* increases, λ_* shifts to the left. Thus, the upper bound of k_t^* occurs when Eq.(10) is tangential to the $Cp - \lambda$ curve, as shown in Fig.4. To characterize this limiting equilibrium point, we linearize Eq.(9) about the equilibrium to obtain

$$\dot{\tilde{\lambda}} = \frac{\rho AR^2 V_w}{2J_e\lambda_*^2}\left(\left.\frac{\partial C_p}{\partial\lambda}\right|_{C_p^*,\lambda_*}\cdot\lambda_* - 3C_p^*\right)\tilde{\lambda}, \quad \tilde{\lambda} = \lambda - \lambda_* \tag{11}$$

Thus, the equilibrium $\left(C_p^*, \lambda_*\right)$ is stable if the slope of the $Cp-\lambda$ curve at that point satisfies

$$\left.\frac{\partial C_p}{\partial \lambda}\right|_{C_p^*,\lambda_*} < \frac{3C_p^*}{\lambda_*} \tag{12}$$

Note from Fig.4 that the region of attraction to the left of λ_*, given by $\lambda_1 < \lambda \leq \lambda_*$, decreases as k_t^* increases. Thus, the robustness of the controller to perturbations in wind speeds decreases with increase in k_t^*. The power extraction is maximized when

$$k_t^* = k_{t,opt} = \rho A R^3 C_{p,opt}/2\lambda_{opt}^3 \tag{13}$$

To maximize the power extraction, the knowledge of $k_{t,opt}$ is necessary. However, it may not be known exactly and may also change with time due to blade erosion, residue buildup etc. Online estimation of $k_{t,opt}$ for power maximization has been addressed in many works such as [5, 7–9], and is not a focus of this paper.

Above Rated Wind Speed - Regime 3

The primary control objective in regime 3 is to deliver a constant rated power, P_{ref}. We propose the following control law and investigate the stability of the resulting closed-loop system obtained from Eq.(7).

$$T_g = P_{ref}/\dot{\theta}_r GR \quad \Rightarrow \quad J_e\ddot{\theta}_r = T_r - P_{ref}/\dot{\theta}_r \tag{14}$$

For constant wind speed operation, as in regime 2, from Eq.(2) we have $\dot{\lambda} = R\ddot{\theta}_r/V_w$. Since $T_r = P/\dot{\theta}_r$, where P is expressed in Eq.(1), we have

$$\dot{\lambda} = \frac{RV_w^2}{J_e\dot{\theta}_r}\left[\frac{1}{2}\rho A C_p - \frac{P_{ref}}{V_w^3}\right] \tag{15}$$

For a constant V_w, the equilibrium condition is

$$\frac{1}{2}\rho A C_p(\lambda_e) = \frac{1}{2}\rho A C_{p,e} = \frac{P_{ref}}{V_w^3} \tag{16}$$

The equilibrium points are shown in Fig.5 Note in Fig.5 that above the rated wind speed, the wind turbine operates at suboptimal rotor efficiencies, i.e. at $C_p < C_{p,opt}$. Hence, the equilibrium condition in Eq.(16) results in two equilibrium points $(C_{p,e}, \lambda_{e,a})$ and $(C_{p,e}, \lambda_{e,b})$. Let $\tilde{\lambda} = \lambda - \lambda_e$. We next consider the dynamics of the error variable $\tilde{\lambda}$ to investigate the stability property of the aforementioned equilibrium points. From Eqs.(15) and (16), we obtain

$$\dot{\tilde{\lambda}} = \frac{1}{2}\rho A \frac{RV_w^2}{J_e\dot{\theta}_r}\left[C_p(\lambda_e+\tilde{\lambda}) - C_p(\lambda_e)\right] \tag{17}$$

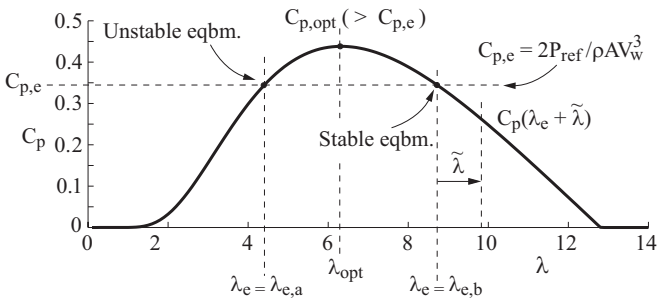

Figure 5. EQUILIBRIUM POINTS FOR ABOVE RATED WIND SPEED UNDER CONTROL LAW EQ.(14)

In Eq.(17), consider the term $\left[C_p(\lambda_e+\tilde{\lambda}) - C_p(\lambda_e)\right]$. Note from Fig. that at the equilibrium point $(C_{p,e}, \lambda_{e,a})$,

$$\left[C_p(\lambda_{e,a}+\tilde{\lambda}) - C_p(\lambda_{e,a})\right] \quad \begin{cases} > 0 \text{ when } 0 < \tilde{\lambda} < (\lambda_{e,b} - \lambda_{e,a}) \\ < 0 \text{ when } \tilde{\lambda} < 0 \end{cases} \tag{18}$$

and at the equilibrium point $(C_{p,e}, \lambda_{e,b})$,

$$\left[C_p(\lambda_{e,b}+\tilde{\lambda}) - C_p(\lambda_{e,b})\right] \quad \begin{cases} < 0 \text{ when } \tilde{\lambda} > 0 \\ > 0 \text{ when } (\lambda_{e,a} - \lambda_{e,b}) < \tilde{\lambda} < 0 \end{cases} \tag{19}$$

Next, considering the following Lyapunov function candidate and its corresponding derivate along the systems trajectories,

$$V = \frac{1}{2}\tilde{\lambda}^2, \quad \dot{V} = \frac{1}{2}\rho A \frac{RV_w^2}{J_e\dot{\theta}_r}\left[C_p(\lambda_e+\tilde{\lambda}) - C_p(\lambda_e)\right]\tilde{\lambda} \tag{20}$$

we observe that for the equilibrium point $(C_{p,e}, \lambda_{e,a})$, $\dot{V} > 0$ for any $\tilde{\lambda} \neq 0$ satisfying $\tilde{\lambda} \in (-\infty, \lambda_{e,b} - \lambda_{e,a})$. Hence from *Chetaev's Theorem* [12], we conclude that $(C_{p,e}, \lambda_{e,a})$ is an unstable equilibrium. For $(C_{p,e}, \lambda_{e,b})$, however, $\dot{V} < 0$ for any $\tilde{\lambda} \neq 0$ satisfying $\tilde{\lambda} \in (\lambda_{e,b} - \lambda_{e,a}, \infty)$. Hence, $(C_{p,e}, \lambda_{e,b})$ is a locally asymptotically stable equilibrium point. Further, for the stable equilibrium point $(C_{p,e}, \lambda_{e,b})$, from the observation above regarding $\dot{V}$ and noting that $\tilde{\lambda}$ moves monotonically toward 0 from either side, we conclude that the domain of attraction is $\lambda \in (\lambda_{e,a}, \infty)$. We end this section by noting that the proposed design does not consider blade pitch variation for attenuating generator torque variations. This will be an area of future research.

Switching Between Regimes 2 and 3

The control laws for regimes 2 and 3 are plotted against $\dot{\theta}_r$ in Fig.6. We propose the switching point between the two regimes to be the intersection where the generator torques are equal. Hence the switching condition and the resulting switch-

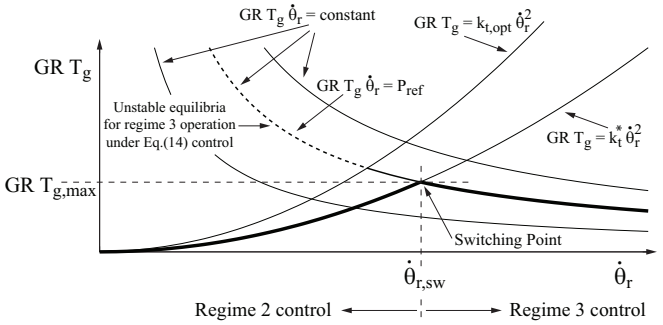

Figure 6. SWITCHING POINT BETWEEN REGIMES 2 AND 3

ing speed are:

$$GR\,T_g = k_t^*\dot{\theta}_r^2 = \frac{P_{ref}}{\dot{\theta}_r} \quad \Rightarrow \quad \dot{\theta}_{r,sw} = \left(\frac{P_{ref}}{k_t^*}\right)^{1/3} \tag{21}$$

Also, note that the control switching point corresponds to the maximum generator torque, $T_{g,max}$. One method to determine $\dot{\theta}_{r,sw}$ and P_{ref} is to use a prescribed $T_{g,max}$ and a regime 2 operating point $\left(C_p^*, \lambda_*\right)$. Then, k_t^* is obtained from Eq.(10) and substituting $T_{g,max}$ and k_t^* in Eq.(21), yields

$$\dot{\theta}_{r,sw} = \left(\frac{GR\,T_{g,max}}{k_t^*}\right)^{1/2} \quad \Rightarrow \quad P_{ref} = k_t^*\dot{\theta}_{r,sw}^3 \tag{22}$$

Alternately, knowing the rated power P_{ref} and k_t^*, one can determine $\dot{\theta}_{r,sw}$ and maximum generator torque $T_{g,max}$ using Eq.(21). Also, note that at the rated wind speed $V_{w,rated}$, the system operates at the switching point $\dot{\theta}_{r,sw}$. Therefore, from the regime 2 operating point $\left(C_p^*, \lambda_*\right)$ and the rated power P_{ref}, $V_{w,rated}$ can be determined using Eq.(1) as follows

$$V_{w,rated} = \left(\frac{2P_{ref}}{\rho A C_p^*}\right)^{1/3} \tag{23}$$

SIMULATIONS

The control strategies developed above were tested using the wind turbine model outlined in Eqs.(3) and (5). The main parameters and their values used for simulation are given below

$$\begin{array}{lll} J_r = 4915797.5 & J_g = 81.2 & GR = 70 \\ D_r = 1000 & D_g = 0.02 & R = 35 \\ K_v = 10 & K_i = 10 & R_g = 0.075 \end{array} \tag{24}$$

The parameter values for J_r, J_g, GR and R were obtained from [13] for a 1.5MW wind turbine. The rest were estimated. In particular, the parameters K_v and K_i were chosen to approximately obtain the rated current and voltages reported in [13]. The parameter R_g was chosen to yield a generator efficiency of $\approx 95-98\%$ at the rated power [2]. The $C_p(\beta,\lambda)$ surface was modeled as the following function

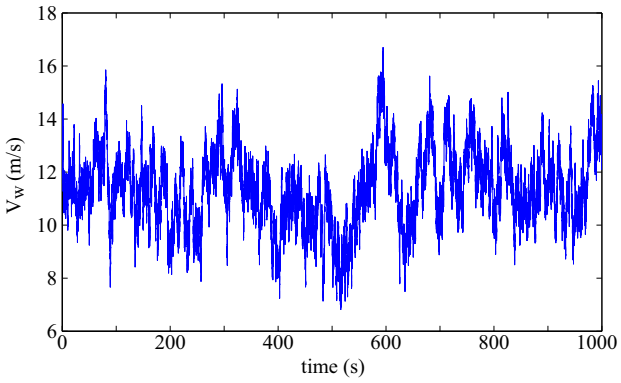

Figure 7. WIND SPEED PROFILE USED FOR SIMULATIONS

$$\begin{aligned} C_p(\beta,\lambda) &= 0.22\left(\tfrac{116}{\lambda_i} - 0.4\beta - 5\right)e^{-\frac{12.5}{\lambda_i}} \\ \tfrac{1}{\lambda_i} &= \tfrac{1}{\lambda+0.08\beta} - \tfrac{0.035}{\beta^3+1} \end{aligned} \tag{25}$$

The surface represented by Eq.(25) is plotted in Fig.1. The calculation of C_p requires blade element theory and Eq.(25) is an approximate analytical solution [14, 15]. The control laws designed in this paper do not assume knowledge of the surface.

In designing the control switching point $\dot{\theta}_{r,sw}$, we consider the pitch angle to be fixed at $\beta = 0$. Note that for the chosen system, $C_{p,opt} = 0.43821$ and $\lambda_{opt} = 6.325$. Thus, from Eq.(13), we have $k_{t,opt} = 1.7502 \times 10^5$. The value of k_t^* is chosen as $k_t^* = 1.5 \times 10^5$ for simulations, which will lead to suboptimal power extraction in regime 2. For power maximization, one of the existing methods for estimating $k_{t,opt}$, such as [5], could be augmented to the basic control in Eq.(8). Thus, from Eq.(21)

$$P_{ref} = 1.5\times10^6\,\text{W},\; k_t^* = 1.5\times10^5 \;\Rightarrow\; \dot{\theta}_{r,sw} = 2.1544\,\text{rad/s} \tag{26}$$

A turbulent wind velocity profile was generated using the *TurbSim* software developed by the National Renewable Energy Laboratory [16]. Wind velocities were generated using an IEC Kaimal Normal Turbulence Model with 12% turbulence intensity and with an average wind speed of 11.32m/s. The average wind speed was chosen equal to the rated wind speed, estimated using Eq.(23) at the rated power $P_{ref} = 1.5$MW and substituting $C_{p,opt} = 0.43821$ for the value of C_p^*. This ensures the wind turbine operates in regimes 2 and 3 for roughly equal amounts of time over the duration of simulation. The generated wind speed data is shown in Fig.7.

The simulation results are shown in Figs.8 and 9. In this simulation, the regime 3 control torque T_g was designed as

$$T_g = \left(P_{ref} + P_{loss}\right)/\dot{\theta}_r GR \tag{27}$$

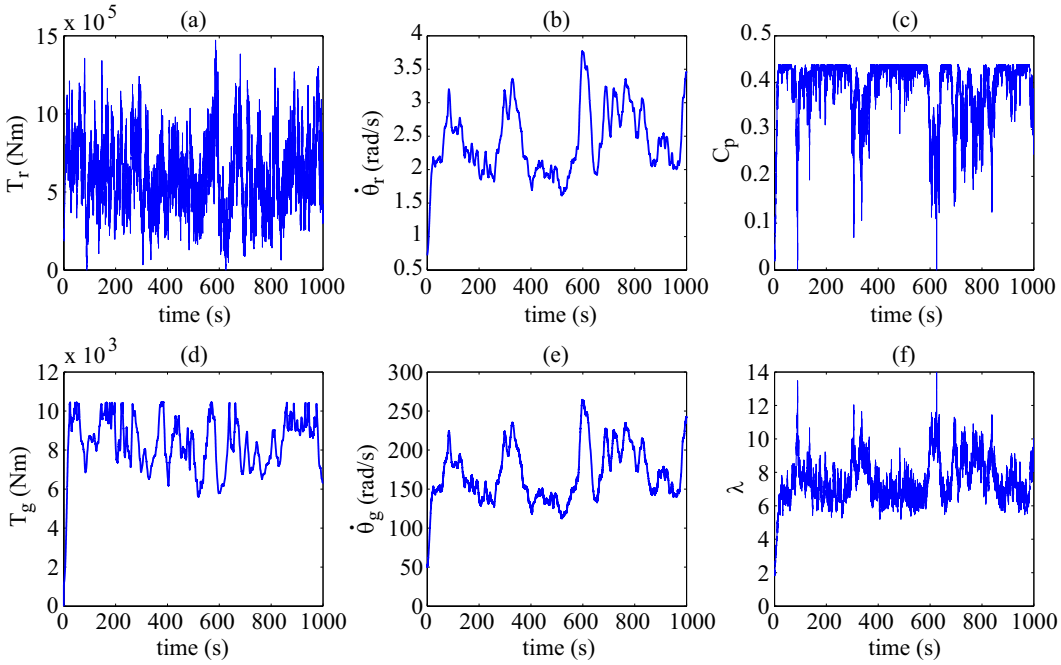

Figure 8. SIMULATION RESULTS FOR COMBINED REGIME 2 AND REGIME 3 OPERATION

instead of Eq.(14), to account for electrical losses. The term $P_{loss} = i_g^2 R_g$, according to our simplified generator model in Eq.(5). Equation (27) assumes the electrical power losses to be known. Figs.8(a), (b), (d) and (e) show the variations in T_r, $\dot{\theta}_r$, T_g and $\dot{\theta}_g$, respectively. Note that T_g is upper bounded due to the control design. The bound can be estimated from Eq.(22) to be $T_{g,max} \approx 10$kNm, which matches with that in Fig.8(d). The C_p and λ plots are given in Figs.8(c) and (f) respectively. The plots show that λ primarily remains confined to the region $\lambda \geq \lambda_{opt}$ with small transient excursions to $\lambda < \lambda_{opt}$. The former region contains the set of stable equilibria for both regimes 2 and 3. In Fig.9(a), we plot the controller state that switches between regimes 2 and 3. In Fig.9(b) we plot the generated power. Comparing Figs.9(a) and (b), we confirm that indeed in regime 3, the rated power is maintained at 1.5MW. Also, from Fig.8(d) and Fig.9(a) we note that there is not abrupt switching of the control input T_g at switching points, as ensured by the control design. In Fig.9(c) we compare the generated power with the mechanical power extracted $T_g\dot{\theta}_g$. The difference is due to the generator losses and can be verified to be around $3-5\%$.

As mentioned earlier, the simulation results presented in Figs.8 and 9 assume a knowledge of the electrical power loss. To compare the effect when the losses are unknown, we run the same simulation, but using Eq.(14) instead of Eq.(27). The results are shown in Fig.10. As expected, without loss compensation the regime 3 power generation is lower. However, the simplicity of the control law, Eq.(14), could outweigh lower extraction, especially if the generator efficiency is high. Nevertheless, the controller of Eq.(14) can be further improved by using feedback to compensate for the losses.

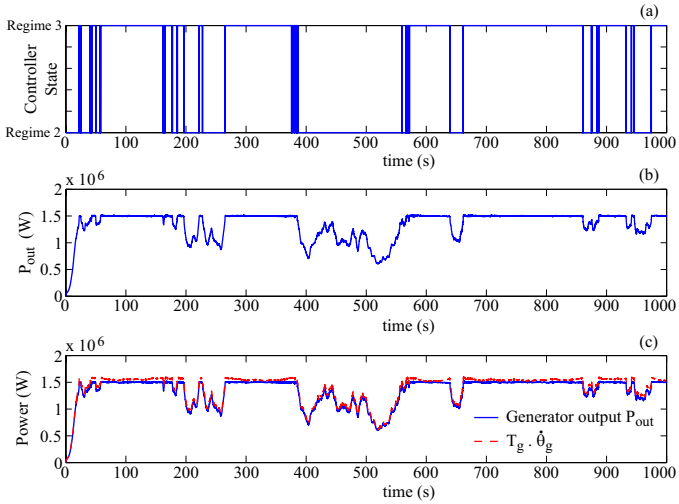

Figure 9. CONTROLLER STATE AND GENERATED POWER

CONCLUSION

We design nonlinear controllers for regime 2 and regime 3 operations of a variable speed wind turbine. For regime 2, we adopt the controller of [5] and provide further insight into the limits of operation under this control law. For regime 3, we propose a simple nonlinear controller. For both regimes, the closed-loop system has two equilibrium points, of which one is shown to be stable. While in regime 2 the stable equilibrium is a fixed point on the (C_p, λ) curve, in regime 3 its location changes with wind speed. Switching between the two regimes is based on the rotor speed whose measurement is assumed available. The control input maintains continuity at the switching point and hence

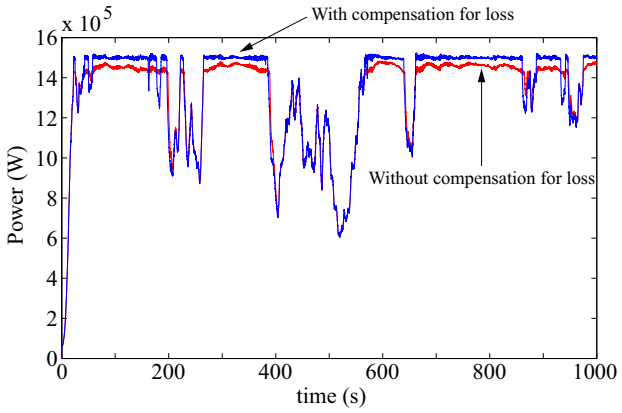

Figure 10. POWER GENERATION WITH AND WITHOUT LOSS COMPENSATION

no jump at the transition point. The controllers and switching mechanisms are validated through simulations. The work presented in this paper can be further improved in two main areas. Firstly, one should analytically investigate if the controller switching could induce instability. Secondly, the regime 3 one could incorporate blade pitch modulation to reduce transients in generator torques. This can potentially be simply augmented to the proposed regime 3 controller.

REFERENCES

[1] Burton, T., Sharpe, D., Jenkins, N., and Bossanyi, E., 2001. *Wind Energy Handbook*, 1st ed. Wiley.

[2] Hodge, B. K., 2009. *Alternative Energy Systems and Applications*. John Wiley & Sons, Inc.

[3] Boukhezzar, B., Lupu, L., Siguerdidjane, H., and Hand, M., 2007. "Multivariable control strategy for variable speed, variable pitch wind turbines". *Renewable,* ***32***, pp. 1273–1287.

[4] Leithead, W. E., and Connor, B., 2000. "Control of variable speed wind turbines: Design task". *International Journal of Control,* ***73***(13), pp. 1189–1212.

[5] Johnson, K. E., Pao, L. Y., Ballas, M. J., and Fingersh, L. J., June, 2006. "Control of variable-speed wind turbines". *IEEE Control Systems Magazine*, pp. 70–81.

[6] Boukhezzar, B., Siguerdidjane, H., and Hand, M., 2006. "Nonlinear control of variable-speed wind turbines for generator torque limiting and power optimization". *ASME Journal of Solar Energy Engineering,* ***128***, pp. 516–530.

[7] Creaby, J., Li, Y., and Seem, J. E., June, 2009. "Maximizing wind turbine energy capture using multi-variable extremum seeking control". *Wind Engineering,* ***33***(4), pp. 361–387.

[8] Hawkins, T., White, W. N., Hu, G., and Sahneh, F. D., September 12-15, 2010. "Wind turbine power capture control with robust estimation". *Proceedings of ASME 2010 Dynamic Systems and Control Conference*.

[9] Iyasere, E., Salah, M., Dawson, D., and Wagner, J., June 11-13, 2008. "Nonlinear robust control to maximize energy capture in a variable speed wind turbine". *American Control Conference, Seattle, Washington*, pp. 1824–1829.

[10] Boukhezzar, B., and Siguerdidjane, H., Toronto, Canada, August 2005. "Nonlinear control of variable speed wind turbines for power regulation". *Proceedings of the IEEE Conference on Control Applications*, pp. 114–119.

[11] Wright, A. D., Fingersh, L. J., and Ballas, M. J., November, 2006. "Testing state-space controls for the controls advanced research turbine". *ASME Journal of Solar Energy Engineering,* ***128***, pp. 506–515.

[12] Khalil, H., 2002. *Nonlinear Systems*, 3 ed. Prentice-Hall, Inc. Upper Saddle River, NJ.

[13] Santoso, S., and Le, H. T., 2007. "Fundamental time-domain wind turbine models for wind power studies". *Renewable Energy,* ***32***, pp. 2436–2452.

[14] Gao, F., Xu, D., and Lv, Y., 2008. "Pitch-control for large-scale wind turbines based on feed forward fuzzy-PI". *Proceedings of the 7th World Congress on Intelligent Control and Automation, June 25-27, Chongqing, China*, pp. 2277–2282.

[15] Slootweg, J. G., Polinder, H., and Kling, W. L., 2001. "Dynamic modeling of a winf turbine with doubly fed induction generator". *IEEE Power Engineering Society Summer Meeting,* ***1***, pp. 644–649.

[16] Kelley, N., and Jonkman, B., 2011. NWTC design codes. http://wind.nrel.gov/designcodes/preprocessors/turbsim/.